Nonlinear subswitching regime of magnetization dynamics in photomagnetic garnets

A. Frej [*], I. Razdolski, A. Maziewski, and A. Stupakiewicz

Faculty of Physics, University of Bialystok, 1L Ciolkowskiego, 15-245 Bialystok, Poland

We analyze, both experimentally and numerically, the nonlinear regime of the photoinduced coherent magnetization dynamics in cobalt-doped yttrium iron garnet films. Photomagnetic excitation with femtosecond laser pulses reveals a strongly nonlinear response of the spin subsystem with a significant increase of the effective Gilbert damping. By varying both laser fluence and the external magnetic field, we show that this nonlinearity originates in the anharmonicity of the magnetic energy landscape. We numerically map the parameter work space for the nonlinear photoinduced spin dynamics below the photomagnetic switching threshold. Corroborated by numerical simulations of the Landau-Lifshitz-Gilbert equation, our results highlight the key role of the cubic symmetry of the magnetic subsystem in reaching the nonlinear spin precession regime. These findings expand the fundamental understanding of laser-induced nonlinear spin dynamics as well as facilitate the development of applied photomagnetism.

I. INTRODUCTION

Recently, a plethora of fundamental mechanisms for magnetization dynamics induced by external stimuli at ultrashort time scales has been actively discussed [1–5]. The main interest is not only in the excitation of spin precession but in the switching of magnetization between multiple stable states, as it opens up rich possibilities for nonvolatile magnetic data storage technology. One of the most intriguing examples is the phenomenon of ultrafast switching of magnetization with laser pulses. Energy-efficient, nonthermal mechanisms of laser-induced magnetization switching require a theoretical understanding of coherent magnetization dynamics in a strongly nonequilibrium environment [6]. This quasiperiodic motion of magnetization is often modeled as an oscillator where the key parameters, such as frequency and damping, are considered within the framework of the Landau-Lifshitz-Gilbert (LLG) equation [1,7]. Although it is inherently designed to describe small-angle spin precession within the linear approximation, there are attempts to extend this formalism into the nonlinear regime where the precession parameters become angle dependent [8]. This is particularly important in light of the discovery of the so-called precessional switching, where magnetization, having been impulsively driven out of equilibrium, ends its precessional motion in a different minimum of the potential energy [6,9–11]. Obviously, such magnetization trajectories are characterized by very large precession angles (usually on the order of tens of degrees). It is, however, generally believed that the magnetization excursion from the equilibrium of about $10°$–$20°$ is already sufficient for the violation of the linear LLG approach [12,13]. Thus, an intermediate regime under the switching stimulus threshold exists, taking a large area

in the phase space and presenting an intriguing challenge in understanding fundamental spin dynamics.

An impulsive optical stimulus often results in a thermal excitation mechanism, inducing concomitant temperature variations, which can impact the parameters of spin precession [14–16]. This highlights the special role of the nonthermal optical mechanisms of switching [17–19]. Among those, we outline photomagnetic excitation, which has been recently demonstrated in dielectric Co-doped yttrium iron garnet (YIG:Co) films [6,11]. There, laser photons at a wavelength of 1300 nm resonantly excite the $^5E \rightarrow {}^5T_2$ electron transitions in Co ions, resulting in an emerging photoinduced magnetic anisotropy and thus in a highly efficient excitation of the magnetic subsystem [6]. This photoinduced effective anisotropy field features a nearly instantaneous rise time (within the femtosecond pump laser pulse duration), shifting the equilibrium direction for the magnetization and thus triggering its large-amplitude precession. In the subswitching regime (at excitation strengths just below the switching threshold), the frequency of the photoinduced magnetization precession has been shown to depend on the excitation wavelength [20]. However, nonlinearities in magnetization dynamics in the subswitching regime have not yet been described in detail, and the underlying mechanism for the frequency variations is not understood.

In this work, we systematically examine the intermediate subswitching regime characterized by large angles of magnetization precession and the nonlinear response of the spin system to photomagnetic excitations. We show a strong increase of the effective Gilbert damping at elevated laser-induced excitation levels (Fig. 1) and quantify its nonlinearity within the existing phenomenological formalism [8]. We further map the nonlinear regime in the phase space formed by the effective photoinduced anisotropy field and the external magnetic field.

This paper is organized in the following order: in the first part, we describe the details of the experiment for laser-

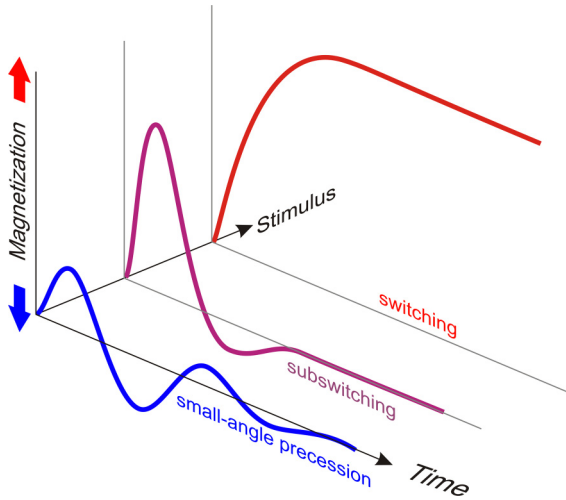*Corresponding author: a.frej@uwb.edu.pl

FIG. 1. Sketch of magnetization dynamics at various stimulus levels. Owing to the highly nonlinear magnetization dynamics in the switching regime, the nonlinearity onset manifests in the subswitching regime too.

induced large-amplitude magnetization precession. Next, we present the experimental results, followed by the fitting analysis. Then, we complement our findings with the results of numerical simulation of the photomagnetic spin dynamics. Afterward, we discuss the work space of parameters for the subswitching regime of laser-induced magnetization precession. The paper ends with conclusions.

II. EXPERIMENTAL DETAILS

The experiments were done on a 7.5 μm thick YIG:Co film with a composition of $Y_2CaFe_{3.9}Co_{0.1}GeO_{12}$. The Fe ions at the tetrahedral and octahedral sites are replaced by Co ions [21]. The sample was grown by liquid-phase epitaxy on a 400 μm thick gadolinium gallium garnet (GGG) substrate. It exhibits eight possible magnetization states along the garnet's cubic cell diagonals due to its cubic magnetocrystalline anisotropy ($K_1 = -8.4 \times 10^3$ erg/cm^3) dominating the energy landscape over the uniaxial anisotropy ($K_u = -2.5 \times 10^3$ erg/cm^3). Owing to the 4° miscut, additional in-plane anisotropy is introduced, tilting the magnetization axes and resulting in slightly lower energy of half of the magnetization states in comparison to the others. In the absence of the external magnetic field, the equilibrium magnetic state corresponds to the magnetization in the domains close to the $\langle 111 \rangle$−type directions in YIG:Co film. Measurements of the Gilbert damping α using the ferromagnetic resonance technique resulted in $\alpha \approx 0.2$. This relatively high damping is inextricably linked to the Co dopants [22–24].

The nonlinearity of an oscillator is usually addressed by varying the intensity of the stimulus and comparing the response of the system under study. Here, we investigated the nonlinear magnetization dynamics by varying the optical pump fluence and, thus, the strength of the photomagnetic effective field driving the magnetization out of the equilibrium. We performed systematic studies in various magnetic states of YIG:Co governed by the magnitude of the external magnetic

fields. The magnetic field $H_\perp$ was applied perpendicular to the sample plane and the in-plane magnetic field H was applied along the [110] direction of the YIG:Co crystal by means of an electromagnet. Owing to the introduced miscut, the studied YIG:Co exhibits four magnetic domains at $H = 0$ [25]. The large jump at an in-plane magnetic field close to zero shows the magnetization switching in the domain structures between four magnetic phases. The optical spot size in this experiment was around 100 μm while the size of smaller domains was around 5 μm, resulting in the spatial averaging of the domains in the measurements. This behavior of magnetic domains was discussed and visualized in detail by the magneto-optical Faraday effect in our previous papers [6,25]. With an increase of the magnetic field up to around $H = 0.4$ kOe, larger and smaller domains are formed due to the domain wall motion, eventually resulting in a formation of a single domain in a noncollinear state. Upon further increase, the magnetization rotates toward the direction of the applied field until a collinear state with in-plane magnetization orientation is reached at about 2 kOe (see Fig. 2).

Dynamic nonlinearities in the magnetic response were studied employing the pump-probe technique relying on the optical excitation of the spin precession in YIG:Co film. The pumping laser pulse at 1300 nm, with a duration of 50 fs and a repetition rate of 500 Hz, induced spin dynamics through the photomagnetic mechanism [6]. The transient Faraday rotation of the weak probe beam at 625 nm was used to monitor the dynamics of the out-of-plane magnetization component M_z. The diameter of the pump spot was around 140 μm, while the probe beam was focused within the pump spot with a size of around 50 μm. The fluence of the pump beam was varied in the range of $0.2-6.5$ mJ/cm^2, below the switching threshold of about 39 mJ/cm^2 [20]. At 1300 nm pump wavelength, the optical absorption in our garnet is about 12%. An estimation of the temperature increase ΔT due to the heat load for the laser fluence of 6.5 mJ/cm^2 results in $\Delta T < 1$ K (see the Methods section of Ref. [6]). The polarization of both beams was linear and set along the [100] crystallographic direction in YIG:Co for the pump and the [010] direction for the probe pulse. The experiments were done at room temperature. At each magnetic field, we performed a series of laser fluence dependent pump-probe experiments measuring the transients of an oscillating magnetization component normal to the sample plane. We then used a phenomenological damped oscillator response function to fit the experimental data and retrieve the fit parameters such as amplitude, frequency, lifetime, and effective damping. In what follows, we analyze the obtained nonlinearities in the response of the magnetic system and employ numerical simulations to reproduce the experimental findings.

III. RESULTS

Time-resolved photomagnetic dynamics

In order to determine the characteristics of the photomagnetic precession, we carried out time-resolved measurements of a transient Faraday rotation $\Delta\theta_F$ in YIG:Co film. Figures 3(a)–3(d) exemplify a few typical datasets obtained for four various pump fluences (between 1.7 and 6.5 mJ/cm^2)
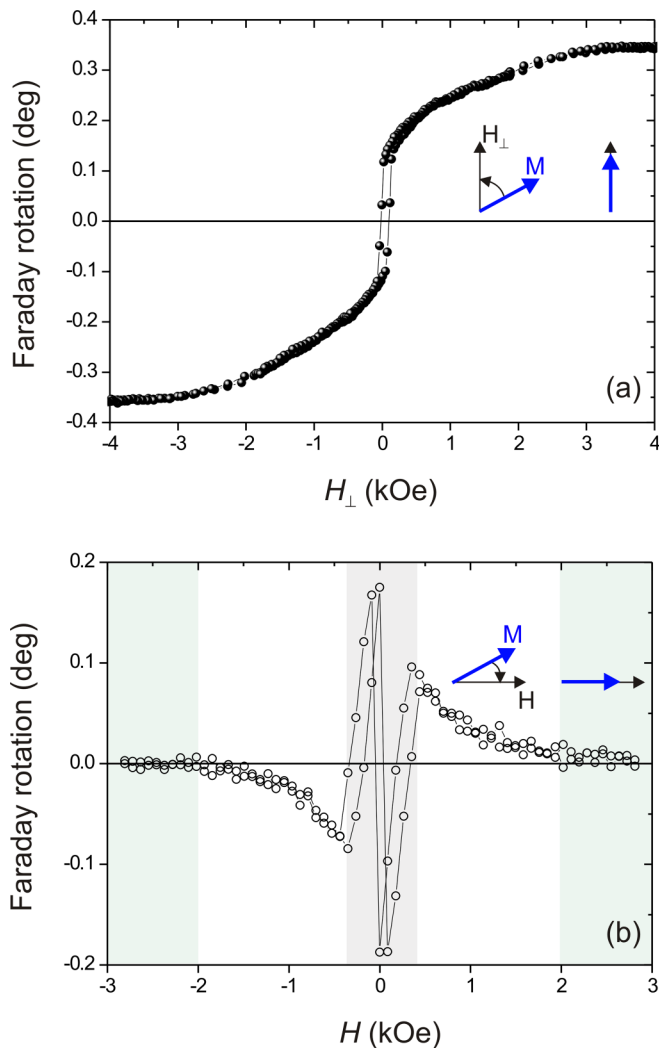
FIG. 2. Magnetization reversal using static magneto-optical Faraday effect under perpendicular $H_\perp$ (a) and in-plane H (b) magnetic fields. The gray area indicates the magnetization switching in magnetic domain structure [25]. The green area shows the saturation range with a collinear state of magnetization.

in magnetic fields of various strengths. A general trend demonstrating a decrease of the precession amplitude and an increase of its frequency is seen upon the magnetization field increase. To get further insights into the magnetization dynamics, these datasets were fitted with a damped sine function on top of a nonoscillatory, exponentially decaying background:

$$\Delta\theta_F(\Delta t) = A_F \sin\left(2\pi f \Delta t + \phi\right)\exp\left(-\frac{\Delta t}{\tau_1}\right)$$
$$+ B\exp\left(-\frac{\Delta t}{\tau_2}\right), \tag{1}$$

where Δt is pump and probe time difference, A_F is the amplitude, f is the frequency, ϕ is the phase, τ_1 is the decay time of precession, and τ_2 is the decay time of the background with an amplitude B.

We note that the fit starts at a time delay of around 60 ps when the photomagnetic effective anisotropy has

already relaxed, and the obtained frequency of the magnetization precession corresponds to the equilibrium state. At low applied fields $H < 1$ kOe, where the photomagnetic anisotropy field (H_L) contribution to the total effective magnetic field is the strongest, the largest magnetization precession amplitude is observed. Figure 4 shows the most important parameters of the magnetization precession, that is, amplitude, frequency, and effective damping [Figs. 4(a)–4(c)]. The latter is obtained from the frequency and the lifetime as $(2\pi f \tau_1)^{-1}$. Although the amplitude dependence on the pump fluence is mostly linear, the other two parameters exhibit a more complicated dependence, which is indicative of the noticeable nonlinearity in the magnetic system. In particular, at $H = 0.4$ and 0.5 kOe, we observed an increase in the effective damping with laser fluence, resulting in a faster decay of the magnetic precession. This is further corroborated by the frequency decrease seen in Fig. 4(b). It is seen that the behavior of the magnetic subsystem is noticeably dissimilar at low (below 1 kOe) and high (above 2 kOe) magnetic fields. At higher magnetic fields $H > 1$ kOe we were unable to observe nonlinear magnetization response at pump fluences up to 10 mJ/cm^2. This is indicative of a significant difference in the dynamic response in the collinear and noncollinear states of the magnetic subsystem.

IV. NONLINEAR PRECESSION OF MAGNETIZATION IN ANISOTROPIC CUBIC CRYSTALS

The data shown in Fig. 4(c) clearly indicate the nonlinearity in the magnetic response manifesting in the increase of the effective damping with the excitation (laser) fluence. Previously, similar behavior was found in a number of metallic systems [26–29] and quickly attributed to laser heating. Interestingly, Chen *et al.* [30] found a decrease of the effective damping with laser fluence in FePt, while invoking the temperature dependence of magnetic inhomogeneities to explain the results. There, the impact of magnetic inhomogeneity driven damping contribution exhibits a similar response to laser heating and an increase in the static magnetic field. A more complicated mechanism relying on the temperature-dependent competition between the surface and bulk anisotropy contributions and resulting in the modification of the effective anisotropy field has been demonstrated in ultrathin Co/Pt bilayers [31,32].

Nonlinear spin dynamics is a rapidly developing subfield enjoying rich prospects for ultrafast spintronics [33]. Importantly, all those works featured thermal excitation of magnetization dynamics in metallic, strongly absorptive systems. In stark contrast, we argue that the mechanism in the Co-doped YIG studied here is essentially nonthermal. This negligible temperature change ΔT is unable to induce significant variations of the parameters in the magnetic system of YIG:Co ($T_N = 450$ K), thus ruling out the nonlinearity mechanism discussed above. Rather, we note the work by Müller *et al.* [34], where the nonthermal nonlinear regime of magnetization dynamics in CrO_2 at high laser fluences was ascribed to the spin-wave instabilities at large precession amplitudes [35]. We also note the recently debated and physically rich mechanisms of magnetic nonlinearities, such as spin inertia [36–39] and relativistic effects [40,41]. Yet, we argue that in
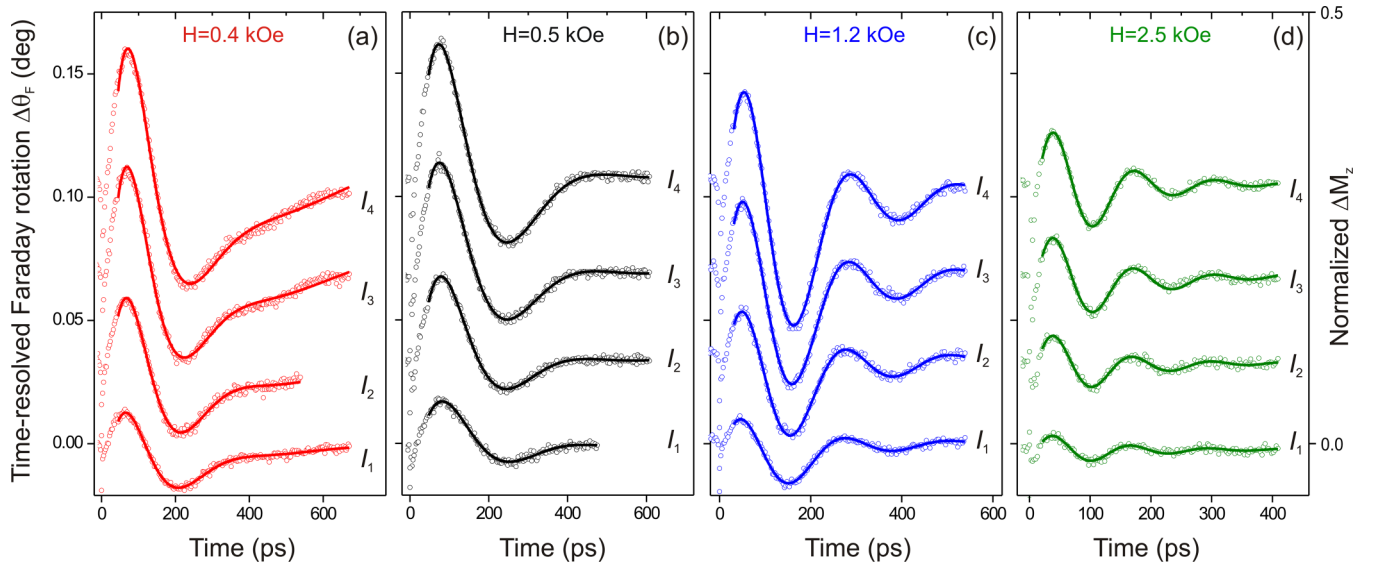
FIG. 3. Time-resolved Faraday rotation at different magnetic fields H (a–d) and laser fluences (I_1–I_4 correspond to 1.7, 3.2, 5.0, and 6.5 mJ/cm^2, respectively). The normalized ΔM_Z on the vertical axis is defined as $\Delta\theta_F/\theta_{\max}$, where $\theta_{\max}$ is obtained for saturation magnetization rotation at $H_\perp$ [see Fig. 2(a)]. The curves are offset vertically without rescaling. The solid lines are fittings with the damped sine function [Eq. (1)].

our case of a cubic magnetic anisotropy dominated energy landscape, a much simpler explanation for the nonlinear spin dynamics can be suggested. In particular, we attribute the amplitude-dependent effective damping to the anharmonicity of the potential well for magnetization.

We performed numerical calculations of the energy density landscape $W(\theta, \varphi)$:

$$W(\theta, \varphi) = W_c + W_u + W_d + W_z, \quad (2)$$

taking into account the following terms in the free energy of the system: the Zeeman energy $W_z = -M \cdot H$, demagnetizing field term $W_d = -2\pi M_s^2 \sin^2\theta$, cubic $W_c = K_1(\sin^4\theta\sin^2\varphi\cos^2\theta + \sin^2\theta\cos^2\theta\cos^2\varphi + \sin^2\theta\cos^2\theta\sin^2\varphi)$,

and uniaxial anisotropy $W_u = K_u\sin^2\theta$ (θ and φ are the polar and azimuthal angles, respectively). In the calculations, we assume $K_1 = -9 \times 10^3$ erg/cm^3, $K_u = -3 \times 10^3$ erg/cm^3, and M_s is the saturation magnetization of 7.2 Oe [25]. Then, following Refs. [8,42], we calculate the precession frequency f and the effective damping α_{eff}:

$$f = \frac{\gamma}{2\pi M_s \sin\theta}\sqrt{\frac{\delta^2 W}{\delta\theta^2}\frac{\delta^2 W}{\delta\varphi^2} - \left(\frac{\delta^2 W}{\delta\theta\delta\varphi}\right)^2}, \quad (3)$$

$$\alpha_{\text{eff}} = \frac{\alpha_0\gamma\left(\frac{\delta^2 W}{\delta\theta^2} + \frac{\delta^2 W}{\delta\varphi^2}\sin^{-2}\theta\right)}{8\pi^2 f M_s}, \quad (4)$$
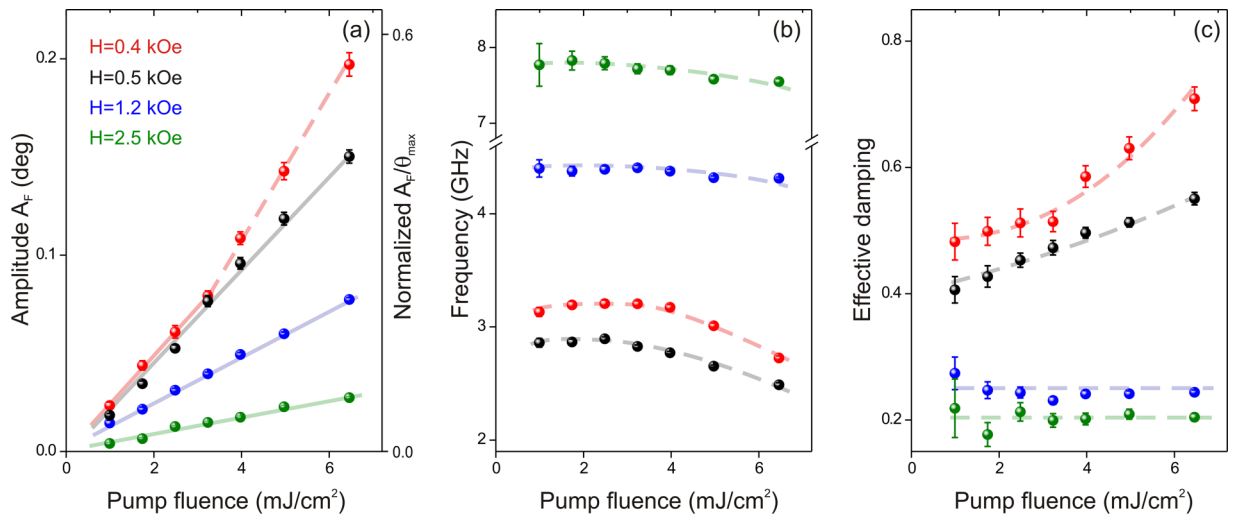

FIG. 4. Photomagnetic precession parameters as a function of pump fluence in different external magnetic field H: (a) amplitude of the Faraday rotation A_F, (b) frequency of the precession, and (c) effective damping. Different colors correspond to different external magnetic fields. The solid lines are the linear fits where applicable, while the dashed lines are the visual guides. Some of the error bars are smaller than the data point symbols.
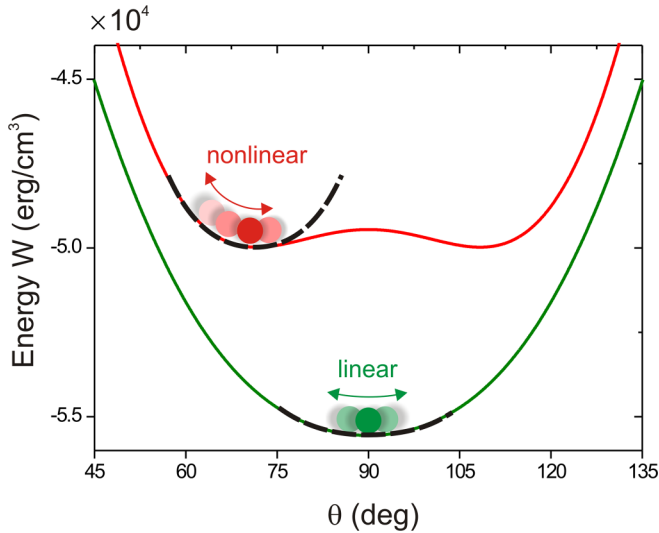
FIG. 5. Energy landscape as a function of the polar angle θ ($\varphi = 45°$) in the linear ($H = 2.5$ kOe, green) and nonlinear ($H = 0.4$ kOe, red) precession regimes. The dashed lines are the parabolic fits in the vicinity of the minima. θ is the polar angle of magnetization orientation measured from the normal to the sample plane along the [001] axis in YIG:Co.
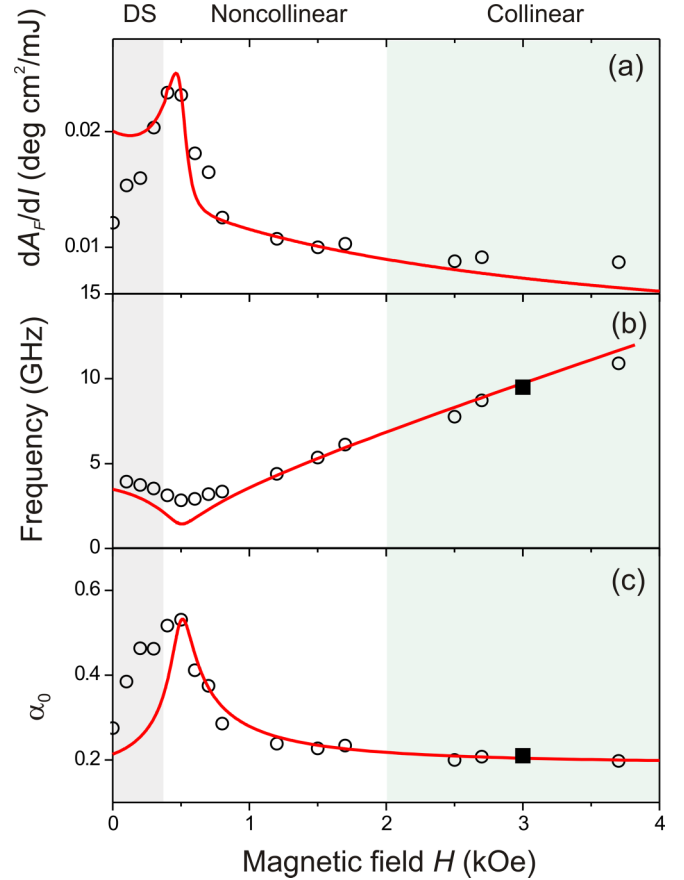

FIG. 6. Photomagnetic precession parameters at various magnetic fields: amplitude (a), frequency (b), and (linear) effective damping (c). The points are from the experimental data; the solid lines are calculated as described in the text. The dark rectangular points are obtained in the ferromagnetic resonance experiments. The gray shaded area indicates the presence of a domain state (DS). The green shaded area shows the magnetization saturation state. The error bars obtained solely from the fitting routine are smaller than the data point symbols.

where the γ is the gyromagnetic ratio and α_0 is the Gilbert damping in YIG:Co [23,24]. In Fig. 5, we only show the total energy as a function of the polar angle θ, to illustrate the anharmonicity of the potential at small external in-plane magnetic fields. Experimental data and calculations of the energy $W(\theta, \varphi)$ have been published in Refs. [25,43]. There, it is seen that at relatively small external magnetic fields canting the magnetic state, the proximity of a neighboring energy minimum (to the right) effectively modifies the potential well for the corresponding oscillator (on the left), introducing an anharmonicity. On the other hand, at sufficiently large magnetic fields,—which, owing to the Zeeman energy term, modify the potential such that a single minimum emerges (shown in Fig. 5 in green)—no nonlinearity is expected. This is also in line with the decreasing impact of the cubic symmetry in the magnetic system, which is responsible for the anharmonicity of the energy potential.

To get yet another calculated quantity that can be compared to the experiment, we introduced the photomagnetically induced effective anisotropy term K_L. This contribution depends on the laser fluence I through the effective light-induced field $H_L \propto I$ as

$$K_L = -2H_L M_s \cos^2 \theta. \tag{5}$$

The presence of this term displaces the equilibrium for net magnetization. The equilibrium directions can be obtained by minimizing the total energy with and without the photomagnetic anisotropy term. Then, knowing the angle between the perturbed and unperturbed equilibrium directions for the magnetization, we calculated the precession amplitude A. We note the difference between the amplitudes A_F, which refers to the Faraday rotation of the probe beam, and A standing for the opening angle of magnetization precession. Although both are measured in degrees, their meaning is different.

Having repeated this for a few levels of optical excitation, we obtained a linear slope of the amplitude vs excitation strength dependence. Figures 6(a)–6(c) illustrate the amplitude, frequency, and (linear) effective damping as a function of the external magnetic field. The agreement between the calculated parameters and those obtained from fitting the experimental data is an impressive indication of the validity of our total energy approach. Further, the linear effective damping value of $\alpha \approx 0.2$ obtained in the limit of strong fields is in good agreement with the values known for our Co-doped YIG from previous works [6,24]. In principle, the effective damping in garnets can increase toward lower magnetic fields. Conventionally attributed to the extrinsic damping contributions, this behavior has been observed in rare-earth iron garnets before as well and ascribed to the generation of the backward volume spin-wave mode by ultrashort laser pulses [44]. It is worth noting that there is no nonlinearity phenomenologically embedded in the approach given above.

Yet, the data presented in Fig. 4(c) indicate the persistent nonlinear behavior of the effective damping. To clarify the
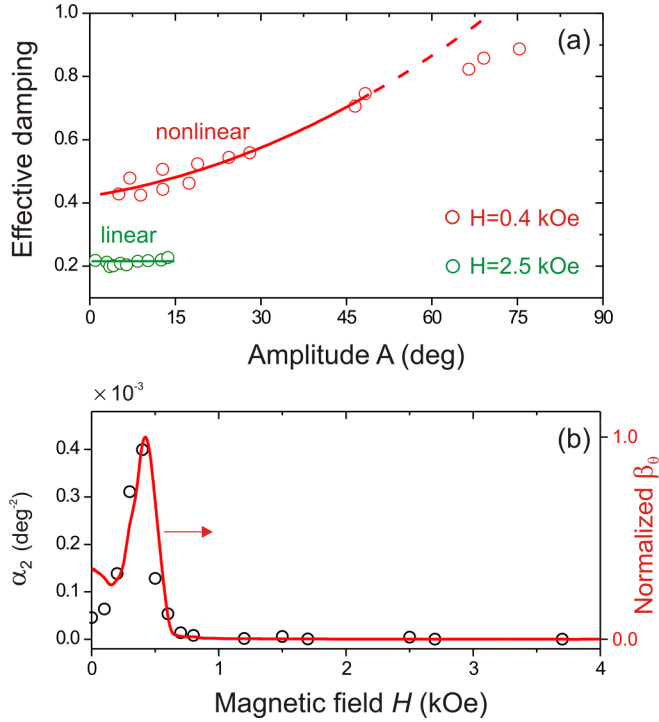
FIG. 7. (a) Effective damping in the linear and nonlinear precession regimes of the precession amplitude A. The lines are the second-order polynomial fits with Eq. (7). (b) Magnetic field dependence of the nonlinearity parameters: nonlinear damping coefficient α_2 (points, obtained from experiments) and the $W(\theta)$ potential anharmonicity normalized β_θ (red line, calculated).

role of the potential anharmonicity, we fitted the potentials $W(\theta, \varphi)$ using a parabolic function with an anharmonic term:

$$W(x) = W_0 + k[(x - x_0)^2 + \beta_x(x - x_0)^4]. \quad (6)$$

Here $x = \theta$ or φ, and β_x is the anharmonicity parameter. We calculated it independently for θ and φ for each dataset of $W(\theta, \varphi)$ obtained at different values of the external magnetic field H by fitting the total energy with Eq. (6) in the vicinity of the energy minimum (Fig. 5). This anharmonicity should be examined on equal footing with the nonlinear damping contribution. To quantify the latter, we follow the approach by Tiberkevich and Slavin [8] and analyze the effective damping dependencies on the precession amplitude by means of fitting a second-order polynomial to them:

$$\alpha = \alpha_0 + \alpha_2 A^2. \quad (7)$$

The examples of the fit curves are shown in Fig. 7(a), demonstrating good quality of the fit within a certain range of the amplitudes A (below 45 °). It should, however, be noted that the model in Ref. [8] has been developed for the in-plane magnetic anisotropy, and thus its applicability for our case is limited. This is the reason why we do not go beyond the amplitude dependence of the effective damping and do not analyze the frequency dependence on A in the limit of strong effective fields. We note that the amplitude A, the opening angle of the precession, should be understood as a mathematical parameter only, and not as a true excursion angle of magnetization obtained in the real experimental conditions. There,

large effective Gilbert damping values and a short decay time of the photomagnetic anisotropy preclude the excursion of magnetization from its equilibrium to reach these A values.

We note that the anharmonicity parameter β_x calculated for the $W(\theta)$ profiles was found to be a few orders of magnitude larger than that obtained for $W(\varphi)$. This difference in the anharmonicity justifies our earlier decision to focus on the shape of $W(\theta)$ potential only (cf. Fig. 5). This means that the potential for magnetization in the azimuthal plane is much closer to the parabolic shape and much larger amplitudes of the magnetization precession are required for it to start manifesting nonlinearities in dynamics. As such, we only consider the anharmonicity β_x originating in the $W(\theta)$ potential energy. In Fig. 7(b), we compare the β_θ (red line) and α_2 (points) dependencies on the external in-plane magnetic field. It is seen that its general shape is very similar, corroborating our assumption that the potential anharmonicity is the main driving force behind the observed nonlinearity. We argue that thanks to the cubic magnetic anisotropy in YIG:Co film, the potential anharmonicity-related mechanism of nonlinearity allows for reaching the nonlinear regime at moderate excitation levels.

V. SIMULATIONS OF LASER-INDUCED MAGNETIZATION DYNAMICS

To further prove that the observed nonlinearities in magnetization dynamics do not require introducing additional inertial or relativistic terms [33], we complemented our experimental findings with numerical simulations of the LLG equation:

$$\frac{d\mathbf{M}}{dt} = -\gamma[\mathbf{M} \times \mathbf{H}_{\text{eff}}(t)] + \frac{\alpha}{M_s}\left(\mathbf{M} \times \frac{d\mathbf{M}}{dt}\right), \quad (8)$$

where H_{eff} is the effective field derived from Eq. (2) as

$$\mathbf{H}_{\text{eff}}(t) = -\frac{\partial W_A}{\partial M} + \mathbf{H}_{\text{L}}(t), \quad (9)$$

We employed the simulation model from Ref. [11] and added a term corresponding to the external magnetic field H. Calculations performed for a broad range of laser fluences and external field values allowed us to obtain a set of traces of the magnetization dynamics. Figure 8 shows a great deal of similarity between simulations and experimental data (cf. Fig. 3). It is seen that the frequency increases with increasing external field H while the amplitude decreases [see Fig. 8(a)]. The simulations for various stimulus strengths show the expected growth of the precession amplitude [see Fig. 8(b)]. The differences, particularly visible for low field time traces, arise from the description complexity of the multimagnetic states in the cubic garnet with a nonzero miscut angle. It should be noted that the purpose of the numerical simulations of the magnetization dynamics presented here was a demonstration of the spin nonlinearity in a system with cubic magnetic symmetry. In doing so, we aimed to obtain a simple and transparent model and minimized the number of model parameters, rather than accurately reproducing the experimental findings.

We further repeated our fit procedure with Eq. (1) to obtain the precession parameters from these data. Figure 9 shows the values of the amplitude and frequency of the precession in the power regime. At a low field $H = 0.4$ kOe (red), the
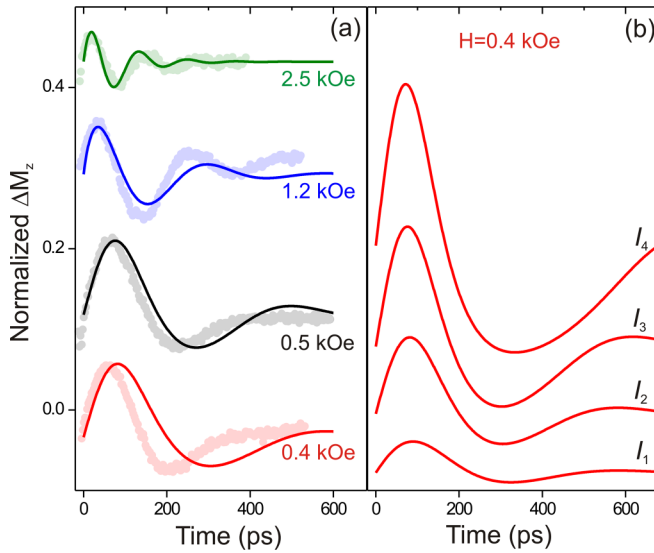
FIG. 8. Photomagnetic precession obtained in numerical simulations of the LLG equation for (a) field dependence at moderate excitation level and (b) power dependence ($I = 4$, 10, 16, and 22 arb. units) at $H = 0.4$ kOe. The dimmed data points are experimental time traces obtained at a laser fluence of 3.2 mJ/cm^2, also shown in Fig. 3.

nonlinearity is clearly visible and comparable with experimental data, as seen in Fig. 4. Similarly, at high fields (green), the behavior is mostly linear. Figure 9(a) shows a great deal of similarity between simulations (amplitude parameter) and experimental data (normalized value $A_F/\theta_{\max}$) [cf. Fig. 4(a)]. The analysis of the damping parameter [Fig. 9(c)] also confirms the experimental findings [as in Fig. 7(a)], revealing the existence of two regimes, linear and nonlinear. The results of the simulations confirm that the observation of the nonlinear response of the magnetic system can be attributed to the anharmonicity of the energy landscape.

Notably, in the simulations, as well as in the experimental data, we not only observe a second-order correction to the effective damping α_2, but also a deviation from Eq. (7) at even larger amplitudes [cf. Figs. 7(a) and 9(c)]. The latter manifests as a reduction of the effective damping compared to the expected $\alpha_0 + \alpha_2 A^2$ dependence shown with dashed lines. This higher-order effect is unlikely to originate in the multimagnon scattering contribution since the latter would only further increase the effective damping [8]. We rather believe that this is likely an artifact of the used damped oscillator model where in the range of $\alpha_{\mathrm{eff}} \approx 1$ the quasiperiodic description of magnetization precession ceases to be physically justified.

VI. PHOTOINDUCED PHASE DIAGRAM OF SUBSWITCHING REGIME

It is seen from both the experimental and numerical results above that the cubic symmetry of the magnetic system is key for the observed nonlinear magnetization dynamics. To quantify the parameter space for the nonlinearity, we first estimate the realistic values of the effective light-induced magnetic field H_L. Throughout a number of works on pho-
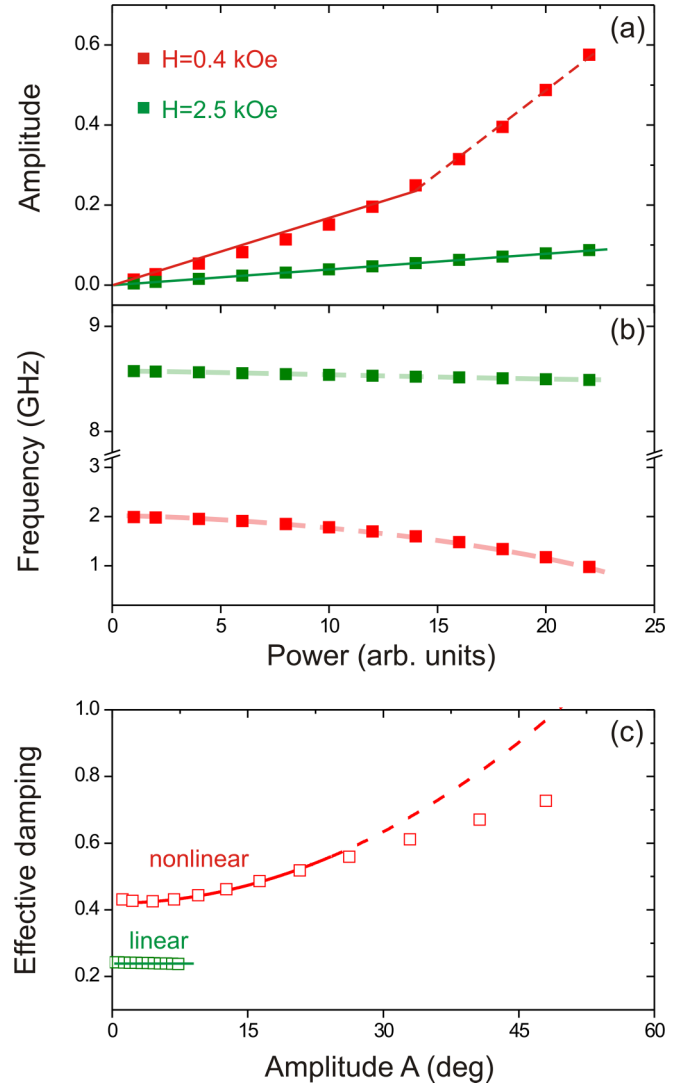

FIG. 9. Power dependence of the (a) amplitude and (b) frequency as obtained in the simulations for low (red dataset) and high (green dataset) external magnetic fields. (c) Effective damping in the linear and nonlinear precession regimes.

tomagnetism in Co-doped garnets, a single-ion approach to magnetic anisotropy is consistently utilized. We note that in YIG:Co, it is the Co ions at tetrahedral sites that are predominantly responsible for the cubic anisotropy of the magnetic energy landscape [22]. In the near-IR range, these ions are resonantly excited at the 1300 nm wavelength, resulting in improved efficiency of the photomagnetic stimulus, as compared to previous works [45]. Further, we note that at the magnetization switching threshold, about 90% of the Co^{3+} ions with a concentration on the order of 10^{20} cm^{-3} are excited with incident photons [11,46]. Taking into account the single-ion contribution to the anisotropy $\Delta K_1 \sim 10^5$ erg/cm^3 [47], and assuming a linear relation between the absorbed laser power (or fluence) and the effective photomagnetic field H_L, for the latter we find that $H_L \sim 1$ kOe is sufficient for the magnetization switching. This means that the subswitching regime of magnetization dynamics (cf. Fig. 1) refers to the
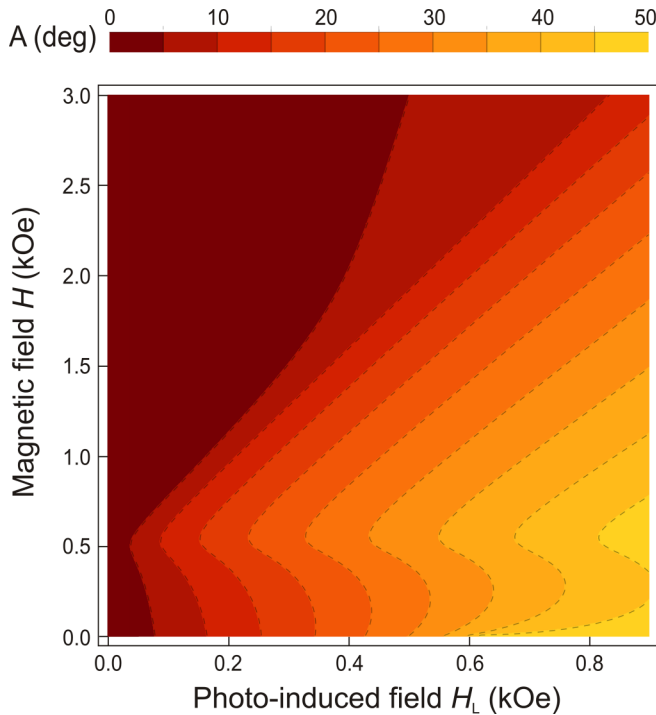
FIG. 10. Calculated amplitude map of the photoinduced magnetization precession in YIG:Co film.

laser fluences (as well as wavelengths), resulting in smaller effective fields.

We reiterate that in previous works, the impact of the external magnetic field on the photomagnetically driven magnetization precession has not been given detailed attention. To address this gap, we plotted the amplitude of the precession A calculated in the same way as above in the subswitching regime (Fig. 10). As expected, the amplitude generally increases with H_L. However, we note a critical external field of about 0.5 kOe at which the desired amplitudes can be reached at smaller light-induced effective fields H_L. At this field, where the system enters a single-domain state, the potential curvature around the energy minimum decreases, thus facilitating the large-angle precession. In other words, external magnetic fields can act as leverage for the effective field of the photoinduced anisotropy, thus reducing the magnetization switching threshold. An exhaustive study of magnetization switching across the parameter space shown in Fig. 10 remains an attractive perspective for future studies.

In our analysis, we only considered a truly photomagnetic excitation and neglected the laser-induced effects of thermal origin. It is, however, known that laser-driven heating can introduce an additional, long-lasting modification of magnetic anisotropy in iron garnets [48,49]. The relatively long relaxation times associated with cooling are responsible for the concomitant modulation of the precession parameters and thus facilitate nonlinearities in the response of the magnetic system. Yet, 1300 nm laser excitation of magnetization dynamics in YIG:Co film was shown to be highly polarization dependent [6], thus indicating the dominant role of the nonthermal excitation mechanism. On the other hand, the unavoidable laser-induced heating with experimental values of laser fluence in YIG:Co film has been estimated to not exceed 1 K [6]. As such, we do not expect modification of the Gilbert damping associated with the proximity of the magnetization compensation or Néel temperature in the ferromagnetic garnet [50]. However, a detailed investigation of the temperature-dependent nonlinear magnetization dynamics in the vicinity of the compensation point or a magnetic phase transition [51,52] represents another promising research direction. Further, exploring the nonlinear regime in the response of the magnetic system to intense THz stimuli along the lines discussed in [33] enjoys a rich potential for spintronic applications.

VII. CONCLUSIONS

In summary, we studied, both experimentally and numerically, the nonlinear regime of magnetization dynamics in photomagnetic Co-doped YIG film. After excitation with femtosecond laser pulses at fluences below the magnetization switching threshold, there is a range of external magnetic field where the magnetic system demonstrates strongly nonlinear precession characterized by a significant increase of the effective Gilbert damping. We attribute this nonlinearity to the anharmonicity of the potential for the magnetic oscillator enhanced by the dominant role of the cubic magnetocrystalline anisotropy. The effective damping and its nonlinear contribution, as obtained from numerical simulations, both demonstrate very good agreement with the experimental findings. Simulations of the magnetization dynamics by means of the LLG equation further confirm the nonlinearity in the magnetic response below the switching limit. Finally, we provide estimations for the realistic, effective photomagnetic fields H_L and map the work space of the parameters in the subswitching, nonlinear regime of photoinduced magnetization dynamics.

[1] A. Kirilyuk, A. V. Kimel, and T. Rasing, Ultrafast optical manipulation of magnetic order, Rev. Mod. Phys. **82**, 2731 (2010).

[2] J. Walowski and M. Münzenberg, Perspective: Ultrafast magnetism and THz spintronics, J. Appl. Phys. **120**, 140901 (2016).

[3] K. Carva, P. Baláž, and I. Radu, Laser-induced ultrafast magnetic phenomena, in *Handbook of Magnetic Materials*, Vol. 26 (Elsevier, Amsterdam, 2017), pp. 29–463.

[4] E. Y. Vedmedenko, R. K. Kawakami, D. D. Sheka, P. Gambardella, A. Kirilyuk, A. Hirohata, C. Binek, O. Chubykalo-Fesenko, S. Sanvito, and B. J. Kirby, The 2020 magnetism roadmap, J. Phys. D: Appl. Phys. **53**, 453001 (2020).

[5] J. Lloyd-Hughes, P. M. Oppeneer, T. Pereira dos Santos, A. Schleife, S. Meng, M. A. Sentef, M. Ruggenthaler, A. Rubio, I. Radu, and M. Murnane, The 2021 ultrafast spectroscopic probes

of condensed matter roadmap, J. Phys.: Condens. Matter **33**, 353001 (2021).

[6] A. Stupakiewicz, K. Szerenos, D. Afanasiev, A. Kirilyuk, and A. V. Kimel, Ultrafast nonthermal photo-magnetic recording in a transparent medium, Nature (London) **542**, 71 (2017).

[7] J. Stöhr and H. C. Siegmann, *Magnetism: From Fundamentals to Nanoscale Dynamics* (Springer, Berlin, 2006).

[8] V. Tiberkevich and A. Slavin, Nonlinear phenomenological model of magnetic dissipation for large precession angles: Generalization of the Gilbert model, Phys. Rev. B **75**, 014440 (2007).

[9] G. V. Astakhov, A. V. Kimel, G. M. Schott, A. A. Tsvetkov, A. Kirilyuk, D. R. Yakovlev, G. Karczewski, W. Ossau, G. Schmidt, L. W. Molenkamp, and T. Rasing, Magnetization manipulation in (Ga,Mn)As by subpicosecond optical excitation, Appl. Phys. Lett. **86**, 152506 (2005).

[10] F. Hansteen, A. Kimel, A. Kirilyuk, and T. Rasing, Femtosecond Photomagnetic Switching of Spins in Ferrimagnetic Garnet Films, Phys. Rev. Lett. **95**, 047402 (2005).

[11] A. Stupakiewicz, K. Szerenos, M. D. Davydova, K. A. Zvezdin, A. K. Zvezdin, A. Kirilyuk, and A. V. Kimel, Selection rules for all-optical magnetic recording in iron garnet, Nat. Commun. **10**, 612 (2019).

[12] A. Baral, S. Vollmar, and H. C. Schneider, Magnetization dynamics and damping due to electron-phonon scattering in a ferrimagnetic exchange model, Phys. Rev. B **90**, 014427 (2014).

[13] D. Afanasiev, I. Razdolski, K. M. Skibinsky, D. Bolotin, S. V. Yagupov, M. B. Strugatsky, A. Kirilyuk, T. Rasing, and A. V. Kimel, Laser Excitation of Lattice-Driven Anharmonic Magnetization Dynamics in Dielectric $FeBO_3$, Phys. Rev. Lett. **112**, 147403 (2014).

[14] E. Carpene, E. Mancini, D. Dazzi, C. Dallera, E. Puppin, and S. De Silvestri, Ultrafast three-dimensional magnetization precession and magnetic anisotropy of a photoexcited thin film of iron, Phys. Rev. B **81**, 060415(R) (2010).

[15] J. A. de Jong, A. V. Kimel, R. V. Pisarev, A. Kirilyuk, and T. Rasing, Laser-induced ultrafast spin dynamics in $ErFeO_3$, Phys. Rev. B **84**, 104421 (2011).

[16] W. He, B. Hu, Q.-F. Zhan, X.-Q. Zhang, and Z.-H. Cheng, Probing nonlinear magnetization dynamics in Fe/MgO(001) film by all optical pump-probe technique, Appl. Phys. Lett. **104**, 142405 (2014).

[17] N. P. Duong, T. Satoh, and M. Fiebig, Ultrafast Manipulation of Antiferromagnetism of NiO, Phys. Rev. Lett. **93**, 117402 (2004).

[18] O. Kovalenko, T. Pezeril, and V. V. Temnov, New Concept for Magnetization Switching by Ultrafast Acoustic Pulses, Phys. Rev. Lett. **110**, 266602 (2013).

[19] V. S. Vlasov, A. M. Lomonosov, A. V. Golov, L. N. Kotov, V. Besse, A. Alekhin, D. A. Kuzmin, I. V. Bychkov, and V. V. Temnov, Magnetization switching in bistable nanomagnets by picosecond pulses of surface acoustic waves, Phys. Rev. B **101**, 024425 (2020).

[20] A. Frej, A. Maziewski, and A. Stupakiewicz, All-optical magnetic recording in garnets using a single laser pulse at *L*-band telecom wavelengths, Appl. Phys. Lett. **118**, 262401 (2021).

[21] S. Geller, Crystal chemistry of the garnets, Z. Kristallogr. - Cryst. Mater. **125**, 1 (1967).

[22] *Landolt-Bornstein Numerical Data and Functional Relationships in Science and Technology*, edited by P. Hansen, K. Enke, and G. Winkler, New Series, Group III, Vol. 12 (Springer-Verlag, Berlin, 1978).

[23] M. Maryško and J. Šimšova, Ferromagnetic resonance study of $Y_{3-z}Ca_zFe_{5-x-y}Co_xGe_yO_{12}$ films, Czech. J. Phys. B **34**, 1125 (1984).

[24] A. Stupakiewicz, M. Pashkevich, A. Maziewski, A. Stognij, and N. Novitskii, Spin precession modulation in a magnetic bilayer, Appl. Phys. Lett. **101**, 262406 (2012).

[25] A. Maziewski, Unexpected magnetization processes in YIG+Co films, J. Magn. Magn. Mater. **88**, 325 (1990).

[26] S. Mizukami, E. P. Sajitha, D. Watanabe, F. Wu, T. Miyazaki, H. Naganuma, M. Oogane, and Y. Ando, Gilbert damping in perpendicularly magnetized Pt/Co/Pt films investigated by all-optical pump-probe technique, Appl. Phys. Lett. **96**, 152502 (2010).

[27] S. Qiao, W. Yan, S. Nie, J. Zhao, and X. Zhang, The in-plane anisotropic magnetic damping of ultrathin epitaxial Co_2FeAl film, AIP Adv. **5**, 087170 (2015).

[28] B. Liu, X. Ruan, Z. Wu, H. Tu, J. Du, J. Wu, X. Lu, L. He, R. Zhang, and Y. Xu, Transient enhancement of magnetization damping in CoFeB film via pulsed laser excitation, Appl. Phys. Lett. **109**, 042401 (2016).

[29] S. Mondal and A. Barman, Laser Controlled Spin Dynamics of Ferromagnetic Thin Film from Femtosecond to Nanosecond Timescale, Phys. Rev. Appl. **10**, 054037 (2018).

[30] Z. Chen, M. Yi, M. Chen, S. Li, S. Zhou, and T. Lai, Spin waves and small intrinsic damping in an in-plane magnetized FePt film, Appl. Phys. Lett. **101**, 222402 (2012).

[31] J. Kisielewski, A. Kirilyuk, A. Stupakiewicz, A. Maziewski, A. Kimel, T. Rasing, L. Baczewski, and A. Wawro, Laser-induced manipulation of magnetic anisotropy and magnetization precession in an ultrathin cobalt wedge, Phys. Rev. B **85**, 184429 (2012).

[32] J. Kisielewski, W. Dobrogowski, Z. Kurant, A. Stupakiewicz, M. Tekielak, A. Kirilyuk, A. V. Kimel, T. Rasing, L. T. Baczewski, A. Wawro, K. Balin, J. Szade, and A. Maziewski, Irreversible modification of magnetic properties of Pt/Co/Pt ultrathin films by femtosecond laser pulses, J. Appl. Phys. **115**, 053906 (2014).

[33] J. Li, C.-J. Yang, R. Mondal, C. Tzschaschel, and S. Pal, A perspective on nonlinearities in coherent magnetization dynamics, Appl. Phys. Lett. **120**, 050501 (2022).

[34] G. M. Müller, M. Münzenberg, G.-X. Miao, and A. Gupta, Activation of additional energy dissipation processes in the magnetization dynamics of epitaxial chromium dioxide films, Phys. Rev. B **77**, 020412(R) (2008).

[35] H. Suhl, The theory of ferromagnetic resonance at high signal powers, J. Phys. Chem. Solids **1**, 209 (1957).

[36] A. V. Kimel, B. A. Ivanov, R. V. Pisarev, P. A. Usachev, A. Kirilyuk, and T. Rasing, Inertia-driven spin switching in antiferromagnets, Nature (London) **5**, 727 (2009).

[37] M. Cherkasskii, M. Farle, and A. Semisalova, Nutation resonance in ferromagnets, Phys. Rev. B **102**, 184432 (2020).

[38] K. Neeraj, N. Awari, S. Kovalev, D. Polley, N. Z. Hagström, S. S. P. K. Arekapudi, A. Semisalova, K. Lenz, B. Green, J.-C. Deinert, I. Ilyakov, M. Chen, M. Bawatna, V. Scalera, M. d'Aquino, C. Serpico, O. Hellwig, J.-E. Wegrowe, M. Gensch,

and S. Bonetti, Inertial spin dynamics in ferromagnets, Nat. Phys. **17**, 245 (2021).

[39] M. Cherkasskii, I. Barsukov, R. Mondal, M. Farle, and A. Semisalova, Theory of inertial spin dynamics in anisotropic ferromagnets, Phys. Rev. B **106**, 054428 (2022).

[40] R. Mondal, M. Berritta, and P. M. Oppeneer, Relativistic theory of spin relaxation mechanisms in the Landau-Lifshitz-Gilbert equation of spin dynamics, Phys. Rev. B **94**, 144419 (2016).

[41] T. G. Blank, K. A. Grishunin, E. A. Mashkovich, M. V. Logunov, A. K. Zvezdin, and A. V. Kimel, THz-scale Field-Induced Spin Dynamics in Ferrimagnetic Iron Garnets, Phys. Rev. Lett. **127**, 037203 (2021).

[42] S. Mizukami, F. Wu, A. Sakuma, J. Walowski, D. Watanabe, T. Kubota, X. Zhang, H. Naganuma, M. Oogane, Y. Ando, and T. Miyazaki, Long-Lived Ultrafast Spin Precession in Manganese Alloys Films with a Large Perpendicular Magnetic Anisotropy, Phys. Rev. Lett. **106**, 117201 (2011).

[43] R. Jabłoński, A. Maziewski, M. Tekielak, and J. Desvignes, FMR study of Co-substituted yttrium iron garnet films, J. Magn. Magn. Mater. **160**, 367 (1996).

[44] S. Parchenko, A. Stupakiewicz, I. Yoshimine, T. Satoh, and A. Maziewski, Wide frequencies range of spin excitations in a rare-earth Bi-doped iron garnet with a giant Faraday rotation, Appl. Phys. Lett. **103**, 172402 (2013).

[45] F. Atoneche, A. M. Kalashnikova, A. V. Kimel, A. Stupakiewicz, A. Maziewski, A. Kirilyuk, and T. Rasing, Large ultrafast photoinduced magnetic anisotropy in a cobalt-substituted yttrium iron garnet, Phys. Rev. B **81**, 214440 (2010).

[46] Z. Šimša, Optical and magnetooptical properties of Co-doped YIG films, Czech. J. Phys. B **34**, 78 (1984).

[47] J. C. Slonczewski, Origin of magnetic anisotropy in cobalt-substituted magnetite, Phys. Rev. **110**, 1341 (1958).

[48] L. A. Shelukhin, V. V. Pavlov, P. A. Usachev, P. Y. Shamray, R. V. Pisarev, and A. M. Kalashnikova, Ultrafast laser-induced changes of the magnetic anisotropy in a low-symmetry iron garnet film, Phys. Rev. B **97**, 014422 (2018).

[49] C. S. Davies, K. H. Prabhakara, M. D. Davydova, K. A. Zvezdin, T. B. Shapaeva, S. Wang, A. K. Zvezdin, A. Kirilyuk, T. Rasing, and A. V. Kimel, Anomalously Damped Heat-Assisted Route for Precessional Magnetization Reversal in an Iron Garnet, Phys. Rev. Lett. **122**, 027202 (2019).

[50] F. Schlickeiser, U. Atxitia, S. Wienholdt, D. Hinzke, O. Chubykalo-Fesenko, and U. Nowak, Temperature dependence of the frequencies and effective damping parameters of ferri-magnetic resonance, Phys. Rev. B **86**, 214416 (2012).

[51] M. Tekielak, A. Stupakiewicz, A. Maziewski, and J. M. Desvignes, Temperature induced phase transitions in Co-doped YIG films, J. Magn. Magn. Mater. **254-255**, 562 (2003).

[52] T. Satoh, Y. Terui, R. Moriya, B. A. Ivanov, K. Ando, E. Saitoh, T. Shimura, and K. Kuroda, Directional control of spin-wave emission by spatially shaped light, Nat. Photonics **6**, 662 (2012).